Experimental and numerical study on the thrust of a water-retaining curtain

Wei He, Jijian Lian, Fang Liu, Chao Ma and Shunqi Pan

ABSTRACT

A water-retaining curtain (WRC) has become a useful facility in selective withdrawal and sedimentation control, but the force analysis of a curved curtain is still lacking. Based on flume experimental tests and numerical simulations, this paper analyzes the variation laws of pressure difference and thrust of WRC. The results show that under the uniform inflow condition, the distribution of pressure difference on the WRC is relatively even, and the maximum value is located at the upper part of the curtain. When arc length–height ratio increases, the location of maximum pressure difference gets lower. In addition, the variation law of thrust of WRC conforms to the classical resistance equation. The drag coefficient is found to fit a power function of the water-retaining ratio, a second-degree polynomial function of arc length–height ratio, and linear function of inclination ratio. The results also yield a simplified forecasting formula of thrust of WRC which is proposed and verified using flume simulations and a real reservoir model test. The newly developed formula systematically considers the water-retaining height, arc length and inclination degree, providing a rapid and accurate algorithm to predict the thrust, and lays a theoretical foundation for practical application.

Key words | drag coefficient, experimental test, numerical simulation, thrust, water-retaining curtain, WRC

Wei He
Jijian Lian (corresponding author)
Fang Liu
Chao Ma
State Key Laboratory of Hydraulic Engineering Simulation and Safety,
Tianjin University,
Tianjin 300072,
China
E-mail: *jjlian@tju.edu.cn*

Shunqi Pan
School of Engineering,
Cardiff University,
The Parade, Cardiff CF24 3AA,
UK

INTRODUCTION

To utilize the water resources, there has been a long history of hydraulic construction all over the world. Traditionally, the rigid hydraulic structures are mainly made of rigid materials such as concrete, steel, cement and rock (Gu & Ouyang 2011; Lin 2015). They have many advantages including high strength, good corrosion resistance, structure stability, and long life. With the development of materials strength and engineering demands, flexible structures have recently been adopted in some hydraulic projects, among which the water-retaining curtain (WRC) is frequently used (Vermeyen 2000; US Department of the Interior 2012). The WRC is made of impermeable flexible materials such as polypropylene fiber geotextile and membrane which has strong mechanical strength and anti-impact ability (Eloy *et al.* 2008; Wang 2010). The main uses of WRC in hydraulic engineering are in the selective withdrawal of reservoirs and sediment trapping, as described below.

To regulate the water temperature discharged from stratified reservoirs, rigid facilities of selective withdrawal are conventionally used including multi-level outlets, stop log gate, side-type orifice intake and surface pumps (Bradford 2000; Zhang & Gao 2010; Wu *et al.* 2013; Gao *et al.* 2014; Soleimani *et al.* 2016). As a flexible facility of selective withdrawal, the WRC is increasingly used to optimize the outflow temperature and water quality due to the advantages of being able to be constructed in an impounded

doi: 10.2166/hydro.2017.095

reservoir, being convenient to be managed, and of much lower cost in comparison with a rigid structure (Asaeda *et al.* 1996, 2001; Vermeyen 1997; Bradford 2000; Bartholow *et al.* 2001). For example, WRCs were implemented to change the outflow temperature to meet the downstream ecological requirements in the Lewiston Reservoir, Holston River and Whiskeytown Reservoir (Boles 1985; Bohac 1989; Vermeyen 2000). Through a WRC flume experiment, Shammaa & Zhu (2010) developed practical relationships to predict the withdrawal composition and the interface height. Lian *et al.* (2016) showed that the outflow temperature was affected by the water-retaining height of a WRC and vertical temperature distribution in the reservoir.

Erosion control of river channels, estuaries and coastal beaches is an important issue all over the world. To solve this problem, many traditional anti-scouring structures have been used, such as artificial bars, seawalls, groins, beach nourishment, breakwaters and vanes (Li & Yu 2009). In recent years, the flexible WRC is proposed and validated in sediment trapping (Li & Yu 2009; Wang *et al.* 2015). The top of a WRC is connected with floaters and the bottom is fixed to the riverbed with strings and anchors, and the curtain is self-adapting to orient with the water flow. Li & Yu (2009) have experimentally analyzed the variation of a floating curtain's oblique angle to the dynamic flow. Wang *et al.* (2014) and Zhu *et al.* (2009) showed that the floating WRC could play a role in flexibility, suspension, movability and diversion, and kept itself stable in the water flow. In summary, a WRC is efficient, and economically and environmentally viable to be constructed and managed in sediment trapping compared with solid structures.

As is clearly shown from the above research and engineering experience, a WRC has shown its advantages including easy construction and modification, convenience in maintenance and low cost. To ensure the safe operation of a WRC, the structure stability of a WRC is noteworthy, and its thrust is a crucial index (Aydin & Demirel 2012; Gallegos *et al.* 2012; Bocchiola & Rosso 2014). A WRC is being designed in the Sanbanxi Reservoir of China to optimize the outflow temperature, and a force analysis of WRC is an imperative focus in the engineering process. Flow around a submerged body is a hot topic in fluid dynamics, and there has been much research on the hydrodynamic characteristics of circular cylinder, square cylinder, river bridge, and pipeline (Fiabane *et al.* 2011; Cheng *et al.* 2012; Turcotte *et al.* 2016; Lou *et al.* 2017). Focusing on a curtain, Wang *et al.* (2014) and Zhu *et al.* (2009) have conducted an experimental study on the tension and stability of a WRC, Wang *et al.* (2015) investigated the inclination angle and pull force of the floating curtain, but the curtain used in the research was rigid and straight rather than curved with only the inclination angle being adjustable. In total, previous research mainly focused on the effectiveness of a curtain in water resource management, and therefore further force analysis of a curved curtain is imperative.

Based on the flume experimental tests and numerical simulations, this paper aims to investigate the pressure difference on the curtain, obtain the change law of drag coefficient and thrust under different curtain forms, and provides technical support for the application. This paper is divided into five sections: the introduction; research methods, including experimental tests and numerical simulations; results wherein the flow field and pressure difference on the WRC are analyzed, and the change law of thrust and drag coefficient is investigated; discussions based on acquired results; and finally, conclusions drawn from the main findings of this research.

METHODS

To quantify the thrust of WRC, the classical resistance equation of cross flow is followed as the theoretical basis for this study. Through experimental tests, the thrust of a WRC is to be obtained, and the numerical simulations can further extract the pressure differences on the curtain.

Preliminary analysis of thrust of WRC

The WRC is subjected to a thrust caused by the water flow, and the thrust comes from the water pressure difference between the upstream and downstream of the curtain, as shown in Figure 1. Depending on a particular engineering application, the curtain can be either set at the top or bottom part of the cross section of a channel. This paper, however, focuses on a bottom-mounted WRC, and

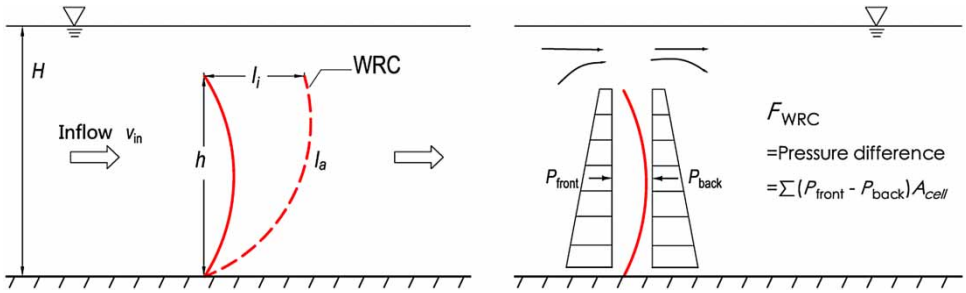

Figure 1 | Sketch of the thrust and arrangement form of a WRC, where v_{in} is inflow velocity, H is water depth, h is water-retaining height, l_a is arc length, l_i is inclination length, F is the force of WRC, P is pressure, and A_{cell} is area of the curtain cells.

the thrust under a uniform inflow condition is studied, as shown in Figure 1. In addition, fresh water is considered in the study, but the effect of sediment on the thrust is ignored.

Considering the force mechanism of WRC is similar to the classical problem of cross flow, the thrust is to be calculated with the resistance equation (Younis *et al.* 2001; Munson *et al.* 2009; Ghadimi & Reisinezhad 2012; Jalonen & Järvelä 2014),

$$f = \frac{F}{B} = \frac{1}{2}\rho v_{in}^2 C_d h \tag{1}$$

where f is the thrust per width (N m^{-1}); F is the time-averaged thrust of WRC (N); B is the flow width (m); v_{in} is the inflow velocity (m s^{-1}); ρ is the fluid density (kg m^{-3}); C_d is the time-averaged dimensionless drag coefficient; and h is the water-retaining height of the WRC (m).

The dimensionless drag coefficient is the key to determining the thrust of WRC, and is thought to be influenced by the curtain forms. Three main influencing factors are considered, which represent the water-retaining degree, curvature and inclination degree of a WRC, respectively, as follows:

1. Water-retaining ratio: $R_h = (h/H)$
2. Arc length–height ratio: $R_a = (l_a/h)$
3. Inclination ratio: $R_i = (l_i/h)$

where H is the water depth (m); l_a is the arc length of curtain (m); l_i is the inclination length of curtain (m), as illustrated in Figure 1.

Experimental test

Model description

Experimental tests are adopted to study hydraulic theories (Jamali *et al.* 2005; Shammaa & Zhu 2010; Sun *et al.* 2016). In this study, a re-circulating rectangular water flume is built, as shown in Figure 2. The flume is 12.5 m long and 2 m wide, and the water depth is 1 m. The inflow velocity and forms of WRC are set according to the model scenarios, as presented in the '*Model scenarios*' section below. The WRC used in the experiments is made of impermeable nylon fabric, and is fixed to the force sensors through fine strings and pulleys. As a flexible material, the curtain is curved in both vertical and lateral directions. Considering the topography of the reservoir, river and estuary, the lateral span of WRC is always much greater than the vertical size. Thus, this paper mainly studies the thrust on a vertically curved curtain. In the span direction, the overall curvature of curtain is kept small although the curvature in some edge areas may be large. The water-retaining height, arc length and inclination length of the curtain can be adjusted by using different forms of curtain. The schematic and arrangement of experimental test are shown in Figure 2.

Test instrument and method

The main instruments used in the experiment include acoustic Doppler velocimetry (ADV), force sensors, dynamic strain gauge, water level sensor system, flow meter and protractor. In the experimental tests, the inflow and outflow flow rates and water level are measured by flow meters

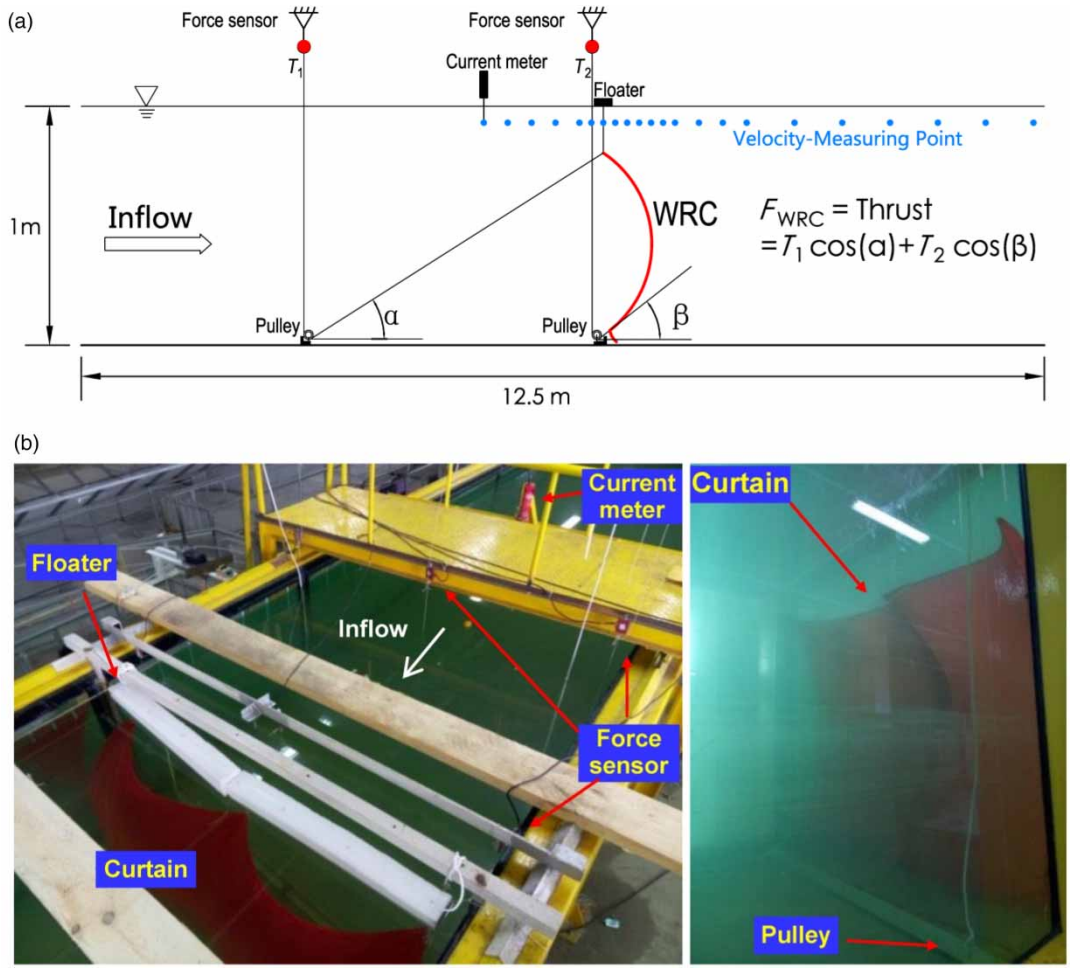

Figure 2 | Description of the experimental test, (a) schematic form and (b) test arrangement.

and water level sensor system, respectively. The longitudinal water velocity along the channel is measured by ADV at multiple locations 0.05 m below the water surface, as shown in Figure 2(a).

There are six force-measuring points on the curtain comprising three bottom points and three top points, and they are connected with force sensors using fine lines and pulleys. Laterally, the force-measuring points are uniformly distributed to make the radiation small, as shown in Figure 2(b). The tensile forces of force-measuring points are measured by force sensors, the angles between fine lines and flow direction are measured through a protractor, and the thrust of WRC is calculated based on the tensile forces and their angles, as shown in Figure 2(a).

Numerical simulations

Model description

The experimental tests can measure the flow field and thrust of WRC, and a numerical simulation based on the common *Fluent* (version 14.5) is set up to further extract the distribution of pressure difference across the curtain (Niedzwiedzka *et al.* 2017). The modeling area and boundary conditions of the numerical model are the same as for the experimental tests. The computational domain is 12.5 m long and 1.2 m high. The water depth is set to 1 m, and the gas-liquid multiphase flow is simulated in the model to ensure the accuracy of the pressure field. Unstructured quadrilateral meshes

are generated and used. According to the magnitude of modeling scope (water: 25×1 m; air: 25×0.2 m) and research priority, considering the computation quantity and accuracy, the average mesh sizes of water and air are determined as 0.02 and 0.04 m, respectively. The numerical values of drag coefficients fit well with observed values in the physical model test, the MAREs are smaller than 5%, indicating that the mesh size is acceptable.

As a flexible body, the WRC is characterized as a large geometric deformation with micro-strain. Similar to the previous research, the experimental tests in this study have shown that the curtain presents a stable geometric deformation under steady flow and tension conditions (Cheng *et al.* 2014; Wang *et al.* 2014). In the numerical model, the WRC is presented with stable wall units, and the coupling effect between curtain and water flow is ignored. The material parameters of WRC are set based on the geotextile characteristics (Frost & Lee 2001; Shi & Li 2016). The bottom boundary of the water channel is set as a wall boundary, and the bottom material is set in line with the experimental test. The upstream and downstream water boundary conditions are set as velocity boundaries, and the air boundary conditions are set as pressure boundaries, as shown in Figure 3.

Governing equations

The 2D model is upon the solution of the incompressible continuity equation and momentum equation, which are expressed as follows:

$$\frac{\partial u_i}{\partial x_i} = 0 \tag{2}$$

$$\frac{\partial(\rho u_j)}{\partial t} + \frac{\partial(\rho u_i u_j)}{\partial x_j} = -\frac{\partial P}{\partial x_j} + \frac{\partial}{\partial x_j}\left(\mu \frac{\partial u_i}{\partial x_j} + \frac{\partial u_j}{\partial x_i}\right) \tag{3}$$

where t is the time (s); x_i and x_j are the co-ordinates (m); u_i and u_j are the velocity components (m s^{-1}); P is the fluid pressure (Pa); μ is the dynamic viscosity coefficient (m^2 s^{-1}).

The two-equation k-ε turbulence model is applied in the 2D model. It is based on the transport equations for turbulent kinetic energy (k; m^2 s^{-2}) and its dissipation rate (ε; m^2 s^{-3}), and is expressed as follows:

$$\frac{\partial}{\partial t}(\rho k) + \frac{\partial}{\partial x_j}(\rho k u_j) = \frac{\partial}{\partial x_j}\left[\left(\mu + \frac{\mu_t}{\sigma_k}\right)\frac{\partial k}{\partial x_j}\right] + G_k - \rho\varepsilon \tag{4}$$

$$\frac{\partial}{\partial t}(\rho \varepsilon) + \frac{\partial}{\partial x_i}(\rho \varepsilon u_i) = \frac{\partial}{\partial x_j}\left[\left(\mu + \frac{\mu_t}{\sigma_\varepsilon}\right)\frac{\partial \varepsilon}{\partial x_j}\right] + \frac{C_{1\varepsilon}\varepsilon}{k} G_k - C_{2\varepsilon}\rho\frac{\varepsilon^2}{k} \tag{5}$$

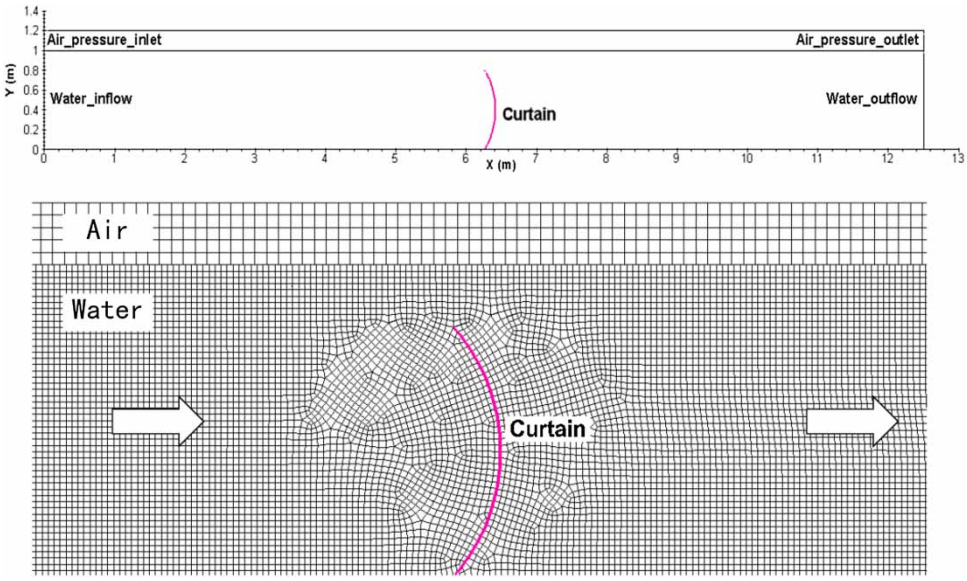

Figure 3 | Meshes and boundary conditions of the numerical model.

where $k = (1/2)u_i'u_j'$ is the turbulent kinetic energy per unit mass, ε is the turbulent energy dissipation rate per unit mass, $\mu_t = \rho C_\mu(k^2/\varepsilon)$ is the kinematic turbulent viscosity, constant C_μ is 0.09, $G_k = \mu_t\left((\partial u_i/\partial x_j) + (\partial u_j/\partial x_i)\right)(\partial u_i/\partial x_j)$ is the production of turbulent kinetic energy from the mean flow, and constants $C_{1\varepsilon}$, $C_{2\varepsilon}$, σ_k and σ_ε are 1.44, 1.92, 1.0 and 1.3, respectively.

The method of volume of fluid is adopted to deal with the free surface problem in the simulation of gas-liquid multiphase flow. The equation for the volume fraction is:

$$\frac{\partial \alpha}{\partial t} + \frac{\partial}{\partial x_i}(u_i\alpha) = 0 \tag{6}$$

where $a \in (0,1)$ is the volume fraction of water, and 1–a represents the volume fraction of air. A cell is full of water (air) at $a = 1$ (0). The mixture properties of fluid, such as density and viscosity, are determined by the volume fraction of water and air, i.e.

$$\rho = \alpha\rho_w + (1-\alpha)\rho_a \tag{7}$$

The finite volume method (FVM) forms the core of the numerical approach by discretization in the solution domain. FVM derives directly from the integral form of the conservation laws for fluid motion and possesses the conservation properties. The pressure-based unsteady implicit method is used in the model solution, and the Pressure Implicit with Splitting of Operators (PISO) scheme is employed in the pressure-velocity coupling. The computational time step is set as 0.0001 seconds. The model simulation time for each scenario is 1,800 seconds, and the CPU (central processing unit) run time is 40–80 hours depending on the flow intensity using a Core i7-3770 3.4 GHz desktop machine. When the changes of time-averaged thrust of WRC and water velocity above WRC are both less than 0.1%, the calculation is judged as convergence. Through numerical simulation, the flow field is simulated, and the time-averaged water velocity and pressure is extracted. Using water pressure upstream and downstream of the curtain, the pressure difference and thrust of the curtain are obtained.

Model scenarios

Currently, a WRC is being designed in the Sanbanxi Reservoir of China to regulate the outflow temperature, and the force estimation of WRC is needed considering different curtain forms. The model scenarios of experimental and numerical simulations are set considering the engineering designation of WRC and hydrological data of Sanbanxi Reservoir (Lian *et al.* 2016; Powerchina ZhongNan Engineering Corporation Limited 2016). The base scenario focuses on the flood releasing at the design standard. In the prototype, the water depth upstream of the dam is approximately 150 m at the flood control level. The outflow discharge of the design standard is 9,600 $m^3\ s^{-1}$, and the corresponding average velocity of the selected cross section is 0.26 $m\ s^{-1}$ (see Appendix, available with the online version of this paper). In the base scenario, the water-retaining proportion of curtain is 80%, and the arc length-height ratio of the curtain is 1.1. The model boundaries of base scenario are converted from the prototype data based on the gravity similarity theory (Munson *et al.* 2009; Lian *et al.* 2015), as shown in Table 1. As the water velocity in the prototype is small, the main factor influencing the thrust of the WRC is the average velocity instead of turbulence. Hence, the similarity of

Table 1 | Description of base scenario

	Water depth (m)	Inflow velocity ($m\ s^{-1}$)	Water-retaining ratio R_h	Arc length–height ratio R_a	Inclination ratio R_i	Bottom roughness
Scale ratio	$\lambda_L = 150$	$\lambda_v = \lambda_L^{1/2} = 12.2$	1	1	1	$\lambda_n = \lambda_L^{1/6} = 2.3$
Prototype	150	0.26	0.8	1.1	0	0.035
Laboratory and numerical models	1	0.02	0.8	1.1	0	0.015

Note: $\lambda_L\lambda_v$ = the length and velocity scale of model, respectively.

average velocity is primarily considered in the model setup, and the similarity of turbulence is currently ignored.

In the base scenario, four boundary variables are considered, including inflow velocity v_{in}, water-retaining ratio R_h, arc length–height ratio R_a and inclination ratio R_i. When one boundary variable changes, the others remain constant. The details of the model scenarios are summarized in Table 2. In the experimental tests and numerical simulations of model scenarios, the boundary conditions are constant, and the time-averaged flow velocity, water pressure, thrust of WRC can be obtained.

In the data analysis and curve fitting of the drag coefficient, the calculated and measured values are both used. The widely used evaluation statistics including mean absolute relative errors (MARE) and coefficient of determination (R^2) are adopted, the former is used to determine the dispersion between measured and calculated values, and the latter is used to present goodness-of-fit equation, as presented in Equations (8) and (9).

$$\mathrm{MARE} = \frac{1}{n}\sum_{I=1}^{n}\frac{\left|X_i^{obs} - X_i^{cal}\right|}{X_i^{obs}} \times 100\% \tag{8}$$

$$\mathrm{R}^2 = \frac{\mathrm{SSR}}{\mathrm{SST}} = 1 - \frac{\mathrm{SSE}}{\mathrm{SST}} = 1 - \frac{\sum_{i=1}^{n}\left(X_i^{obs} - X_i^{sim}\right)^2}{\sum_{i=1}^{n}\left(X_i^{obs} - X^{mean}\right)^2} \tag{9}$$

where n is the total number of observations, $X_i{}^{obs}$ is the ith observed value, $X_i{}^{\mathrm{cal}}$ is the ith calculated or fitted value, X^{mean} is the mean of observed values, SST is the sum of squares for total, SSR is the sum of squares for regression, and SSE is the sum of squares for error.

RESULTS

Through experimental tests and numerical simulations, the hydrodynamic characteristics are investigated, the pressure difference and thrust of WRC are extracted, and the results are described in detail in the following sections.

Flow field

Taking the base scenario (A0) as an example, the flow field near the WRC is extracted and analyzed. In the upstream of

Table 2 | Model scenarios of physical tests and numerical simulation

Number	Description	Inflow velocity v_{in} (m s^{-1})	Water-retaining ratio R_h	Arc length–height ratio R_a	Inclination ratio R_i
A0	Base scenario	0.02	0.8	1.1	0
A1	Varying inflow velocities v_{in}	0.005	0.8	1.1	0
A2		0.0075	0.8	1.1	0
A3		0.01	0.8	1.1	0
A4		0.03	0.8	1.1	0
A5		0.05	0.8	1.1	0
A6	Varying water-retaining ratios R_h	0.02	0.9	1.1	0
A7		0.02	0.6	1.1	0
A8		0.02	0.4	1.1	0
A9	Varying arc length–height ratios R_a	0.02	0.8	1	0
A10		0.02	0.8	1.05	0
A11		0.02	0.8	1.2	0
A12		0.02	0.8	1.3	0
A13	Varying inclination ratios R_i	0.02	0.8	1.1	0.25
A14		0.02	0.8	1.1	0.5
A15		0.02	0.8	1.1	1
A16		0.02	0.8	1.1	1.5

the curtain, the flow field hardly changes along the channel. Near the curtain, the water column in the lower layer upwells, the water column is rapidly contracted to the flow area above WRC, and the flow field looks like a jet flow, as shown in Figure 4. Downstream of the curtain, owing to the upwelling of water column, the jet flow zone initially contracts and then gradually expands, and there is a large recirculation zone below the jet flow zone. The flow field under the setup of the curtain is similar with that of flow over a submerged cylinder, sill and pipelines (Sabag *et al.* 2000; Jamali & Haddadzadegan 2010; Mudgal & Pani 2012; Inverno *et al.* 2016).

The flow velocity above the curtain tends to be very large, and can impose a significant influence on the arrangement of hydraulic structures. For the flow above the curtain, the longitudinal velocity of the water surface along the channel is extracted, as shown in Figure 5. The flow velocity above the curtain rapidly increases initially and then slowly decreases, and the maximum flow velocity appears at the location about 0.3 m downstream the curtain. Hence, instead of exactly above the curtain, the maximum flow velocity of water surface appears somewhere downstream of the curtain, which should be noticed in practice.

Pressure difference and thrust of WRC

Effect of inflow velocity

Through numerical simulation, the longitudinal pressure differences on the WRC are extracted, as shown in Figure 6. Under the scenarios of different inflow velocities v_{in}, vertical distributions of longitudinal pressure difference are, in general, similar. From the bottom to the top of the curtain, the pressure difference first slowly increases and then rapidly decreases near the top of the curtain. The maximum pressure difference is located at the upper part of the curtain (approximately 95% from the bottom). In terms of magnitude, the maximum pressure difference is approximately 1.04 times of the average value, and the coefficient of dispersion is 0.09. In summary, the distribution of pressure difference on the WRC is relatively homogeneous. The reason is that the inflow velocity is uniform, thus making the distribution of pressure difference even.

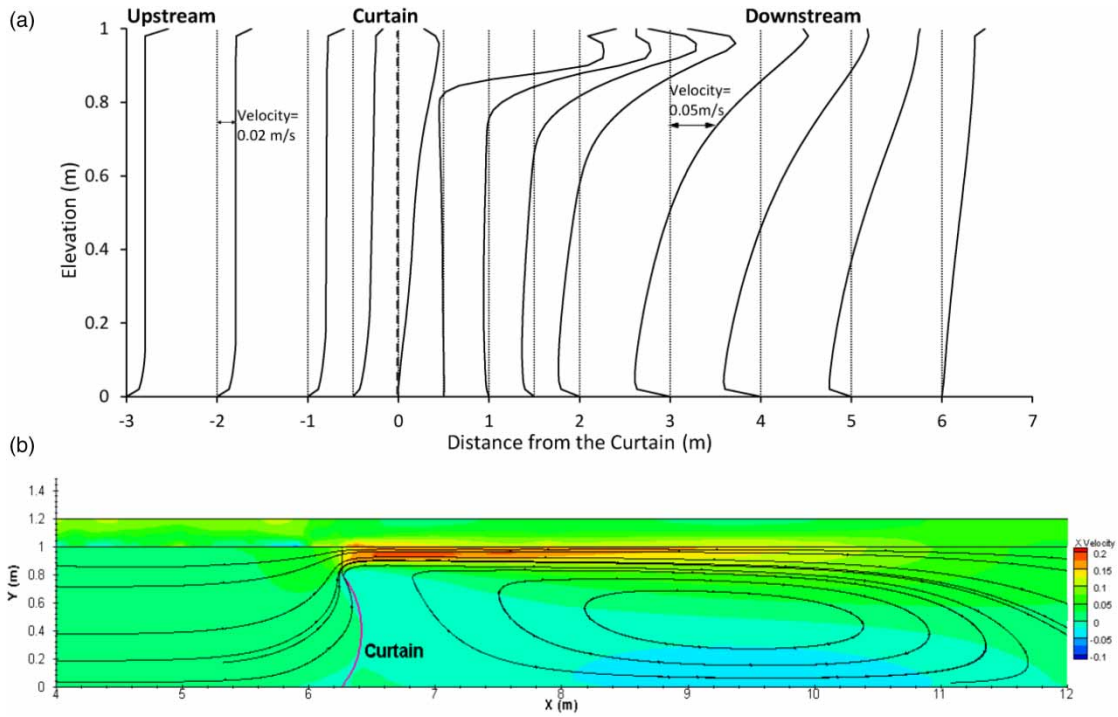

Figure 4 | Flow field near the curtain for Scenario A0 showing (a) longitudinal flow velocity along the channel and (b) contour and streamlines of flow velocity.

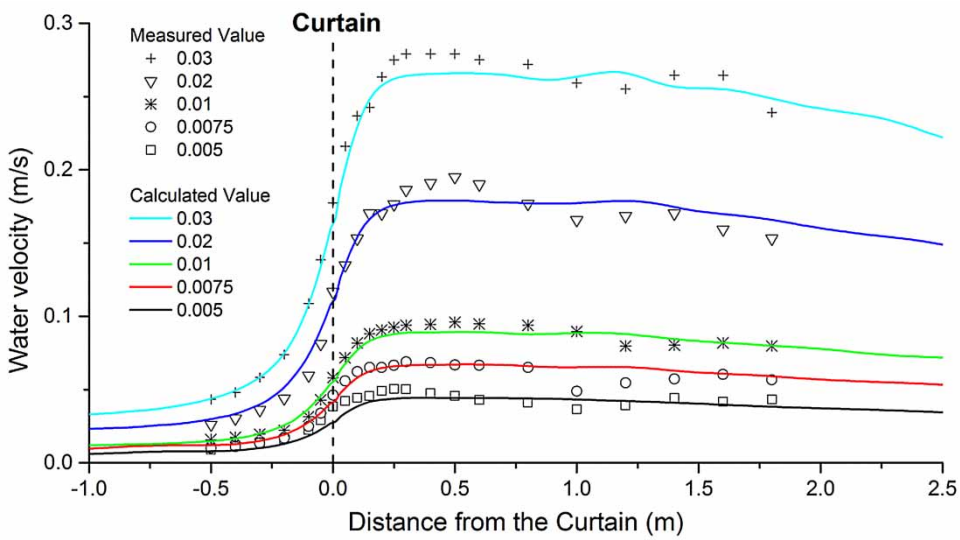

Figure 5 | Longitudinal velocity of water surface along the flume channel under different inflow velocities v_{in} (m s^{-1}).

The calculated and measured thrusts of WRC and the corresponding drag coefficients are shown in Figure 7. The thrust of the curtain rapidly grows as v_{in} increases. Drag coefficients under different inflow velocities are in the range 77.5–82. The MARE between calculated and measured drag coefficients is 2.1%. When the inflow velocity is large, the drag coefficients are all close to 79, but when the inflow velocity is small, the measured drag coefficients show some dispersion. This may be due to the frictional forces between the lines and pulleys which can cause large errors when inflow velocity and resulting thrust are small. In general, the variation range of drag coefficient under different inflow velocities is small, as shown in Figure 7(b).

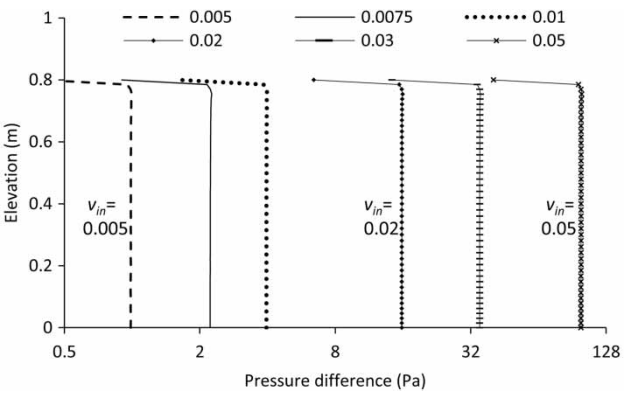

Figure 6 | Vertical distributions of pressure difference under different inflow velocities (m s^{-1}).

Effect of water-retaining ratio

Under scenarios of different water-retaining ratios R_i, the vertical distributions of longitudinal pressure difference are similar, as shown in Figure 8. The locations of maximum pressure difference are at about 95% of the upper curtain. In terms of magnitude, when the water-retaining ratio increases from 0.4 to 0.9, the pressure difference on the curtain gets much larger. The water-retaining ratio imposes a large impact on the magnitude of pressure difference. A larger water-retaining height will significantly contract the water flow, and make the flow field near the curtain change more drastically, as a result, the pressure difference caused by water flow rapidly increases.

The calculated and measured thrusts of WRC and the corresponding drag coefficients are shown in Figure 9. The thrust and drag coefficient rapidly increase as the water-retaining ratio increases, and their changes are in agreement with the variation rule of power fitting. The MARE between calculated and measured drag coefficients is 2.8%. The drag coefficients under different water-retaining ratios are in the range 5.5–333.2, which means that the water-retaining ratio has a different influence on the drag coefficient. With the increase in the water-retaining ratio, not only does the impact area of curtain increase, but also the flow area above WRC gets smaller and the flow field near the curtain changes more drastically, so the thrust and drag coefficient caused by water flow rapidly

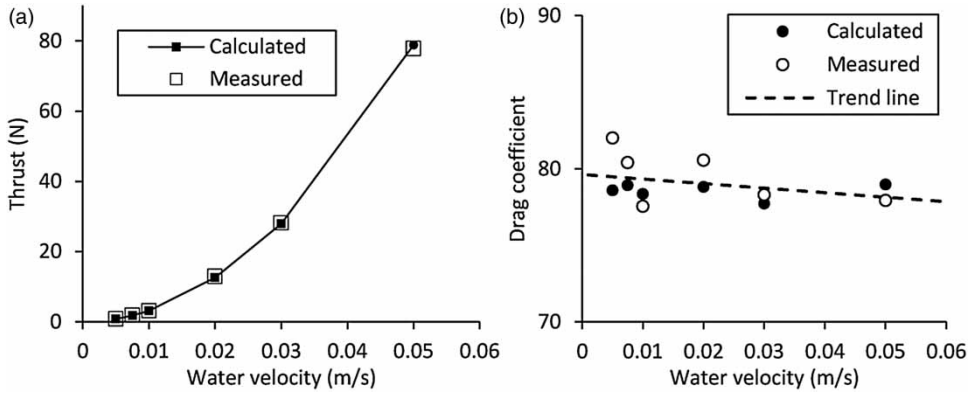

Figure 7 | (a) Thrust and (b) drag coefficients of the WRC under different inflow velocities.

increases. Using both the calculated and measured values of drag coefficients, a fitting formula is obtained to quantify the influence of the water-retaining ratio on the drag coefficient, as shown in Figure 9(b).

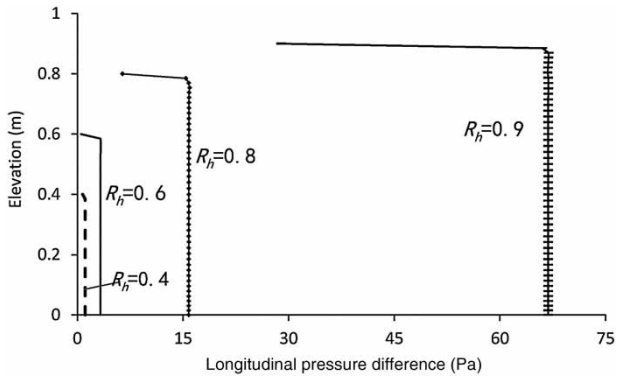

Figure 8 | Vertical distributions of pressure difference under different water-retaining ratios.

Effect of arc length–height ratio

Under different arc length–height ratios, R_a, the vertical distributions of longitudinal pressure difference are distinguishable, as shown in Figure 10. From the bottom to the top of the curtain, when R_a is larger than 1.1, the pressure difference increases first and then decreases. However, when R_a is smaller than 1.1, the pressure difference presents a trend of decrease–increase–decrease upwards. Within the range of R_a from 1 to 1.3, the location of maximum pressure difference moves down from 95% to 75% height of the curtain from the bottom. The reason for the change of the pressure difference distribution may be as follows. The longitudinal pressure difference is the product of pressure difference and its longitudinal vector. Owing to the curved shape of the curtain, the longitudinal vector of water pressure in the upper part of curtain is smaller than

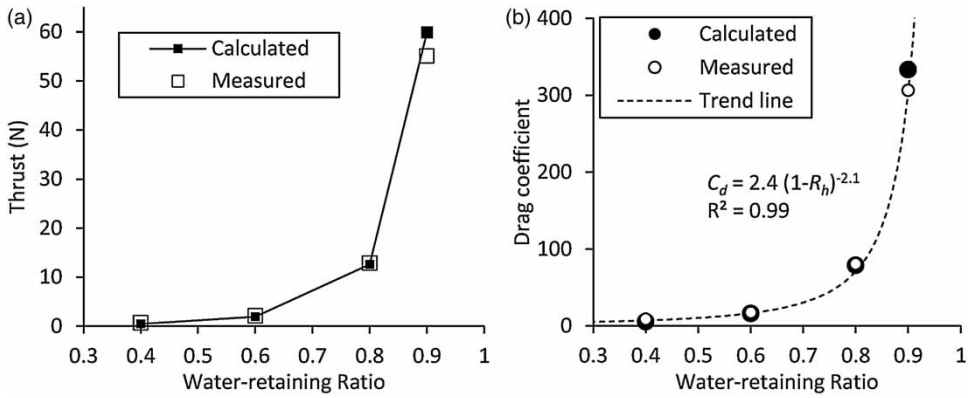

Figure 9 | (a) Thrust and (b) drag coefficients under different water-retaining ratios.

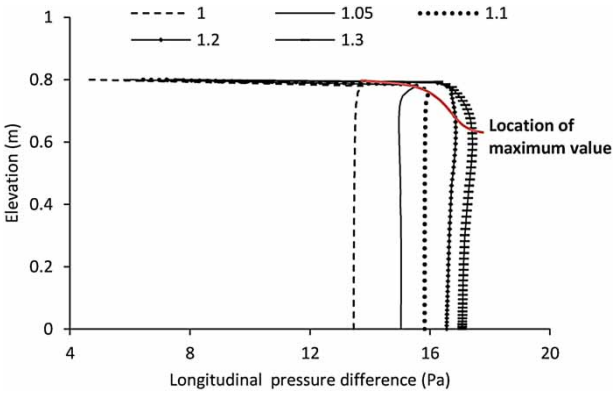

Figure 10 | Vertical distributions of pressure difference under different arc length–height ratios.

that in the middle part (approximately 1). When R_a increases, the curvature of WRC increases, the longitudinal vector in the middle part keeps unchanged, and the longitudinal vector in the upper part gets smaller. Thus, under the combined influence of water pressure and longitudinal vector, the maximum pressure difference will move down.

In terms of magnitude, the pressure difference increases under a larger R_a. When R_a increases, the curtain is bending backwards, the flow field near the curtain changes more drastically, and the pressure difference gets larger.

The calculated and measured thrusts of the curtain and the corresponding drag coefficients are shown in Figure 11. The thrust and drag coefficient nonlinearly grow as R_a increases, and its change accords with the variation rule of second-degree polynomial fitting. Using both the calculated and measured values of drag coefficients, a fitting formula is obtained to quantify the influence of arc length–height ratio on the drag coefficient, as shown in Figure 11(b).

Effect of inclination ratio

Under scenarios of different curtain inclination ratios R_i, the vertical distributions of longitudinal pressure difference are similar, as shown in Figure 12. The locations of maximum pressure difference on the WRC are at about 95% of the curtain. In terms of magnitude, as the inclination ratio increases from 0 to 1.5, the pressure difference on the curtain gets smaller. When the curtain inclination ratio R_i increases, the flow field near the curtain changes more moderately, and hence the pressure difference reduces.

The calculated and measured thrusts and the corresponding drag coefficients are shown in Figure 13. As the flow field near the curtain changes more moderately, the thrust and drag coefficient synchronously decrease when R_i increases, and their changes are in accord with variation rule of linear fitting. Using both the calculated and measured values of drag coefficients, a linear fitting formula is obtained to quantify the influence of inclination ratio on the drag coefficient, as shown in Figure 13(b).

Formula of thrust of WRC

A fast quantization method of thrust is very useful and necessary for the application of WRC, especially in case of emergency, such as sudden heavy rains or large inflow

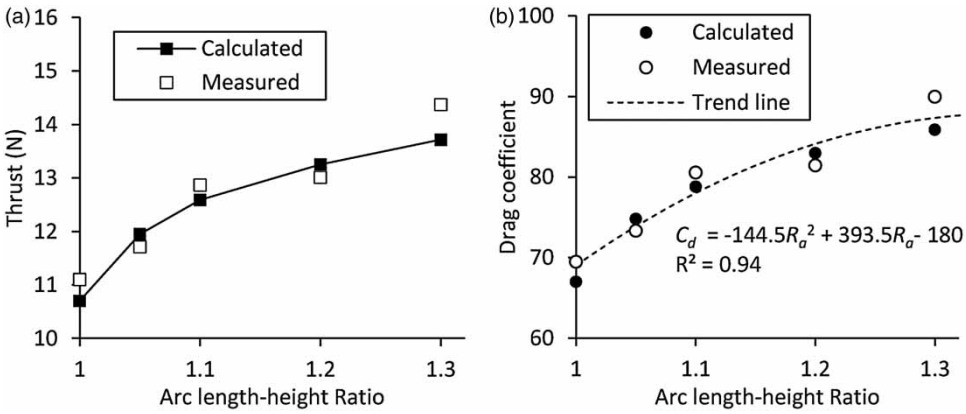

Figure 11 | (a) Thrust and (b) drag coefficients under different arc length–height ratios.

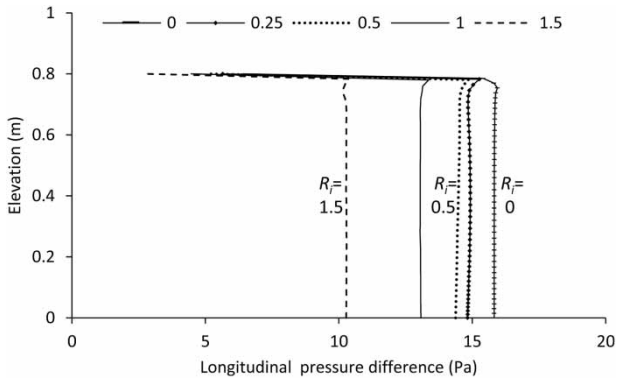

Figure 12 | Vertical distributions of pressure difference under different inclination ratios.

events. Based on the results above, the influence the curtain has on the thrust and drag coefficient is investigated, and a simplified formula of thrust is proposed and verified using flume simulations and a real reservoir model test, which are described below.

Proposition of formula

From the results presented above, the influence of different boundary variables on the drag coefficient of WRC is obtained, and their sensitivity analysis is shown in Table 3. Evidently, the influence degree of various variables is water-retaining ratio > inclination ratio > arc length–height ratio > inflow velocity, and the drag coefficient is barely affected by the inflow velocity. In combination with the results of flow field, the flow characteristics over a WRC are similar to the classical problem of cross flow, and the thrust of the curtain matches with the resistance equation (Equation (1)).

Through curve fitting, the drag coefficient is found to be a power function with water-retaining ratio R_h, a second-degree polynomial function with arc length–height ratio R_a and linear function with inclination ratio R_i, the fitting equation is shown in Figures 9(b), 11(b) and 13(b). Systematically considering the variation trend of thrust and dimensionless drag coefficient under different curtain forms, a fitting calculation is applied to find the simplified approximate formula. Three main characteristic variables representing the form parameter of WRC are used, including arc length–height ratio R_a, water-retaining ratio R_h and inclination ratio R_i. Together with the resistance equation (Equation (10)), the simplified forecasting formula of drag coefficient and thrust is shown below.

$$f = \frac{F}{B} = \frac{1}{2}\rho v_{in}^2 C_d h \tag{10}$$

$$C_d = C(R_h, R_a, R_i) = 79.5 f(R_h) f(R_a) f(R_i) \tag{11}$$

$$f(R_h) = \frac{2.4(1 - R_h)^{-2.1}}{79.5} \tag{12}$$

$$f(R_a) = \frac{-144.5R_a^2 + 393.5R_a - 180.0}{79.5} \tag{13}$$

$$f(R_i) = \frac{-19.9R_i + 80.9}{79.5} \tag{14}$$

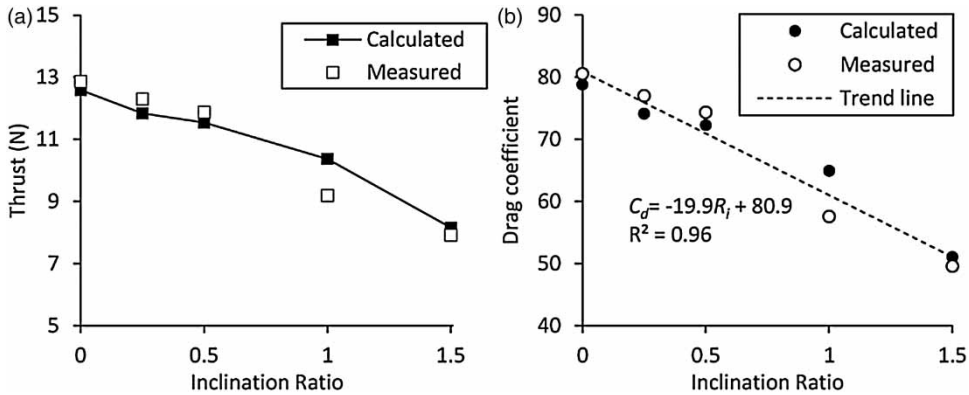

Figure 13 | (a) Thrust and (b) drag coefficients under different inclination ratios.

Table 3 | Sensitivity analysis of different boundary variables

Parameter	Change	Drag coefficient and the relative change
Baseline	–	79.5
Inflow velocity	+50%	78.0 (−2%)
	−50%	78.0 (−2%)
Water-retaining ratio	+12.5%	319.8 (+02%)
	−25%	16.8 (−79%)
Arc length–height ratio	+10%	68.3 (−14%)
	−10%	82.5 (+4%)
Inclination ratio	+0.5	73.3 (−8%)
	+1	61.2 (−23%)

where v_{in} is the inflow velocity (m s^{-1}), H is the water depth (m), h is the water-retaining height (m), $R_h = (h/H)$ is the water-retaining ratio, $R_h \in (0.4,0.9)$, l_a is the arc length of curtain (m), $R_a = (l_a/h)$ is the arc length–height ratio, $R_a \in (1,1.3)$, l_i is the inclination length of curtain (m), and $R_i = (l_i/h)$ is the inclination ratio, $R_i \in (0,1.5)$.

Verification using flume simulations

Firstly, the proposed forecasting formula of thrust is verified using flume simulations described above. The thrusts under various boundary conditions are calculated using flume numerical simulations and forecasting formula. Boundary conditions are set as various combinations of inflow velocities (0.005, 0.001, 0.02, 0.05 m s^{-1}), arc length–height ratios (1.1, 1.2, 1.3), water-retaining ratios (0.2, 0.4, 0.6) and inclination ratios (0, 0.5, 1), a total of 108 sets. Calculated thrusts are shown in Figure 14. Results from forecasting formula coincide well with the results from flume simulations with MARE and R^2 being 13% and 0.97, respectively.

Verification using a real reservoir model test

Secondly, taking Sanbanxi Reservoir as an example, the forecasting formula of thrust is verified using a real reservoir model test. A hydraulic physical model of the Sanbanxi Reservoir was built, and a detailed description of the physical model is presented in the Appendix (available with the online version of this paper). The water-retaining ratios of WRC are set to 45%, 67% and 76%, and the outflow discharges are 4,870, 9,600 and 14,100 m^3 s^{-1}, respectively. The thrusts are obtained

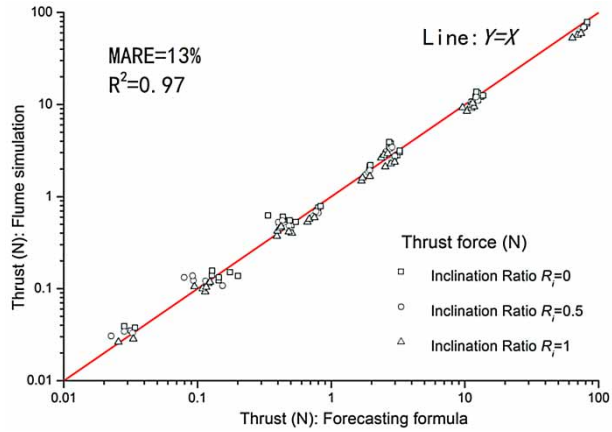

Figure 14 | Comparison of thrusts calculated by flume simulations and forecasting formula.

using Sanbanxi Reservoir experiments and forecasting formula, as shown in Figure 15. Results calculated from the forecasting formula match well with the results from the Sanbanxi Reservoir experiment, the values for MARE and R^2 are 14% and 0.96, respectively. In total, the flume simulations and Sanbanxi Reservoir experiments show a good practicability and accuracy of the proposed forecasting formula.

DISCUSSION

This research has studied the influence of curtain forms on the pressure difference and thrust of WRC, and proposed a forecasting formula of thrust and drag coefficient. The results are further discussed on the following aspects.

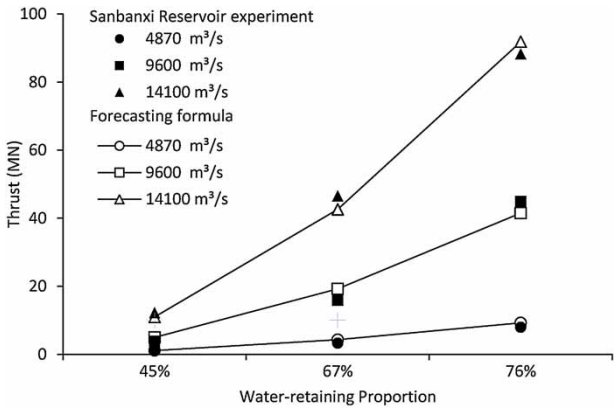

Figure 15 | Comparison of thrusts calculated by Sanbanxi Reservoir experiments and forecasting formula.

The first point regards the application of the forecasting formula of thrust. On one hand, the study of this paper is based on the experimental research of a rectangular flume. While in the practical engineering, the shape of flow cross section of most deep canyon reservoirs and natural river channels tends to be irregular. In the calculation of dimensionless drag coefficient C_d, the water-retaining ratio should be the area ratio of the curtain to the cross section, rather than the ratio of water-retaining height to the water depth. In addition, this formula is obtained under the condition of uniform inflow velocity, and the influence of inflow velocity irregularity on the result should be noted. Qualitatively, when averaged velocity is the same, the thrust is expected to be smaller if the inflow velocity in the upper layers gets larger. In the follow-up study, a force analysis of WRC under different inflow distributions should be developed.

The second point is about the designation of form of WRC. This paper has quantified the influence of arrangement form of the curtain on the thrust of WRC, the thrust of WRC is significantly smaller when water-retaining height decreases or inclination length increases. However, from an engineering viewpoint, the water-retaining effect under a curtain which is vertical and higher would be better, i.e., the degree of improvement of water temperature and quality of vertical curtain is better. Thus in the designation and implementation of a curtain, both the thrust and engineering aspects should be considered to determine the arrangement form of the curtain. The internal stress of WRC is another noteworthy issue concerning the safety and stability of the structure. Regarding hydrodynamic force on the curtain, the thrust of the curtain increases by 9% when the arc length–height ratio increases from 1.1 to 1.3. But with respect to structural internal stress, the curvature of the curtain decreases under a smaller arc length–height ratio, and in turn the internal tensile force of the curtain would be very large even though the hydrodynamic force is small. Thus, a longer arc length will decrease the structural internal stress and increase the robustness of the curtain system. The arc length should be determined comprehensively considering the hydrodynamic force and structural internal stress. In a further study, a finite element analysis of the internal stress of the curtain would be conducted to provide more accurate technical support for the curtain system stability.

The third point is about the application and generalization of WRC. So far, the curtain has been used in selective withdrawal from reservoirs and sedimentation control, and its application can be further extended in other fields. On the one hand, the curtain can be used to store freshwater in estuaries, coasts and rivers, acting as a newly developed coastal reservoir (Yang & Lin 2011; Liu *et al.* 2013) or traditional rubber dam. On the other hand, the curtain can also be used as a good carrier of water purifiers or biofilms in the river channel to improve water quality (Carpenter & Helbling 2017; Li *et al.* 2017). With the development of material strength and construction technology, the flexible curtain would be economic, environmentally sound and conveniently constructed, managed, dismantled and moved in the two examples above.

Meanwhile, there are certain limitations and prospects to our study. Firstly, because the control of a flexible curtain in the experimental tests is harder than that of a rigid structure, there are unavoidably some systematic errors in the experimental tests, i.e. there is spanwise radian in edge areas of the curtain, and there also exists frictional forces between the lines and pulleys which can influence the measured thrust of WRC, especially when the thrust is small. Secondly, this paper mainly studied the effect of vertical radian on the thrust, and the effect of radian in a spanwise direction on the thrust can be further studied, and a 3-D model can be developed. Thirdly, the fitting calculation is mainly applied to find the simplified approximate formula, and the physical mechanism about the influence of different factors should be further investigated.

CONCLUSIONS

In this study, both numerical modeling and laboratory experiments are used to investigate the influence of curtain forms on the pressure difference and thrust of WRC, and a forecasting formula is proposed and verified. This study shows the following: There is a large recirculation zone behind the WRC, and the maximum flow velocity of the water surface appears at a certain location downstream of the curtain; the distribution of pressure difference on the curtain is relatively uniform, and the maximum value is located at the upper part of the curtain. When arc length–height ratio increases, the

location of maximum pressure difference moves downwards; the variation of thrust of WRC conforms to the classical resistance equation. The drag coefficient changes little under different inflow velocities. Increasing water-retaining height and arc length, and reducing curtain inclination ratio will result in an increase of the drag coefficient. The drag coefficient is a power function with the water-retaining ratio, a second-degree polynomial function with the arc length–height ratio and a linear function with the inclination ratio; and finally, forecasting formula of thrust of WRC is proposed and verified using both flume simulations and Sanbanxi Reservoir experiments. This formula has systematically considered the water-retaining height, arc length and inclination degree, which is practical and convenient for the prediction of thrust.

The results presented in this paper can be further utilized in fields related to other materials like membrane, sheet and plate. With the increasing use of flexible materials in hydraulic engineering and other fields, this research can be extended to include flexible structures in future research.

ACKNOWLEDGEMENTS

This research was supported by the National Key Research and Development Program of China (2016YFC0401708), Program of Introducing Talents of Discipline to Universities (B14012), and National Natural Science Foundation of China (51609167). The authors acknowledge the assistance of anonymous reviewers.

REFERENCES

Asaeda, T., Priyantha, D. G. N., Saitoh, S. & Gotoh, K. 1996 A new technique for controlling algal blooms in the withdrawal zone of reservoirs using vertical curtains. *Ecological Engineering* **7**, 95–104.

Asaeda, T., Pham, H. S., Nimal Priyantha, D. G., Manatunge, J. & Hocking, G. C. 2001 Control of algal blooms in reservoirs with a curtain: a numerical analysis. *Ecological Engineering* **16**, 395–404.

Aydin, I. & Demirel, E. 2012 Hydrodynamic modeling of Dam-Reservoir response during earthquakes. *Journal of Engineering Mechanics-ASCE* **138**. doi.org/10.1061/(ASCE)EM.1943-7889.0000322.

Bartholow, J., Hanna, R. B., Saito, L., Lieberman, D. & Horn, M. 2001 Simulated limnological effects of the Shasta Lake temperature control device. *Environmental Management* **27**, 609–626.

Bocchiola, D. & Rosso, R. 2014 Safety of Italian dams in the face of flood hazard. *Advances in Water Resources* **71**, 23–31.

Bohac, C. 1989 Underwater Dam and embayment aeration for striped bass refuge. *Journal of Environmental Engineering* **2**, 428–446.

Boles, G. L. 1985 *Water Temperature and Control in Lewiston Reservoir for Fishery Enhancement at Trinity River Hatchery in Northern California*. California Department of Water Resources, Red Bluff, CA.

Bradford, S. 2000 *Scoping Options for Mitigating Cold Water Discharges From Dams*. CSIRO Land and Water, Canberra.

Carpenter, C. M. G. & Helbling, D. E. 2017 Removal of micropollutants in biofilters: hydrodynamic effects on biofilm assembly and functioning. *Water Research* **120**, 211–221.

Cheng, X., Wang, G. & Wang, Y. 2012 Hydrodynamic forces on a large pipeline and a small pipeline in piggyback configuration under wave action. *Journal of Waterway, Port, Coastal, and Ocean Engineering* **138**, 394–405.

Cheng, C., Tan, W. & Liu, L. 2014 Numerical simulation of water curtain application for ammonia release dispersion. *Journal of Loss Prevention in the Process Industries* **30**, 105–112.

Eloy, C., Lagrange, R., Souilliez, C. & Schouveiler, L. 2008 Aeroelastic instability of cantilevered flexible plates in uniform flow. *Journal of Fluid Mechanics* **611**, 97–106.

Fiabane, L., Gohlke, M. & Cadot, O. 2011 Characterization of flow contributions to drag and lift of a circular cylinder using a volume expression of the fluid force. *European Journal of Mechanics – B/Fluids* **30**, 311–315.

Frost, J. D. & Lee, S. W. 2001 Microscale study of geomembrane-geotextile interactions. *Geosynthetics International* **8**, 577–597.

Gallegos, H. A., Schubert, J. E. & Sanders, B. F. 2012 Structural damage prediction in a high-velocity urban dam-break flood: field-scale assessment of predictive skill. *Journal of Engineering Mechanics-ASCE* **138**, 1249–1262.

Gao, X., Li, G. & Han, Y. 2014 Effect of flow rate of side-type orifice intake on withdrawn water temperature. *Scientific World Journal* 979140. doi: 10.1155/2014/979140.

Ghadimi, P. & Reisinezhad, A. 2012 Numerical simulation of flood waves and calculation of exerted forces on the cylindrical piers in contraction channels with different cross section profiles. *Journal of Hydroinformatics* **14**, 366–385.

Gu, X. & Ouyang, L. 2011 Study of the durability characteristics of hydraulic concrete. *Key Engineering Materials* **477**, 393–397.

Inverno, J., Neves, M. G., Didier, E. & Lara, J. L. 2016 Numerical simulation of wave interacting with a submerged cylinder using a 2D RANS model. *Journal of Hydro-Environment Research* **12**, 1–15.

Jalonen, J. & Järvelä, J. 2014 Estimation of drag forces caused by natural woody vegetation of different scales. *Journal of Hydrodynamics, Ser. B* **26**, 608–623.

Jamali, M. & Haddadzadegan, H. 2010 Effects of a sill on selective withdrawal through a point sink in a linearly stratified fluid. *Advances in Water Resources* **33**, 1517–1523.

Jamali, M., Seymour, B. & Kasaiian, R. 2005 Numerical and experimental study of flow of a stratified fluid over a sill towards a sink. *Physics of Fluids* **17**, 0571065.

Li, Y. & Yu, G. 2009 Experimental investigation on flow characteristics at leeside of suspended flexible curtain for sedimentation enhancement. *China Ocean Engineering* **23**, 565–576.

Li, J., Li, Y., Qian, B., Niu, L., Zhang, W., Cai, W., Wu, H., Wang, P. & Wang, C. 2017 Development and validation of a bacteria-based index of biotic integrity for assessing the ecological status of urban rivers: a case study of Qinhuai River basin in Nanjing, China. *Journal of Environmental Management* **196**, 161–167.

Lian, J., He, W., Ma, C. & Xu, K. 2015 Guarantee rate of freshwater in a river mouth intruded by saltwater with respect to the joint impact of runoff and tide. *Journal of Hydroinformatics* **17**, 917–929.

Lian, J., Du, H. & Ma, C. 2016 Effects of temperature control curtain on water releases in deep water reservoirs. *Journal of Hydraulic Engineering* **47**, 942–948. (In Chinese)

Lin, J. 2015 *Hydraulic Structures.* China Water & Power Press, Beijing, China.

Liu, J., Yang, S. & Jiang, C. 2013 Coastal reservoirs strategy for water resource development-a review of future trend. *Journal of Water Resource and Protection* **5**, 336–342.

Lou, X., Zhou, T. & Cheng, L. 2017 Hydrodynamic coefficients of a yawed square cylinder in oscillatory flows. *Ocean Engineering* **130**, 510–522.

Mudgal, B. V. & Pani, B. S. 2012 Drag characteristics of Two-Dimensional sills in forced hydraulic jumps. *Journal of Hydraulic Engineering* **5**, 462–466.

Munson, B. R., Young, D. F., Okiishi, T. H. & Huebsch, W. W. 2009 *Fundamentals of Fluid Mechanics.* John Wiley & Sons, London, UK.

Niedzwiedzka, A., Lipinski, S. & Kornet, S. 2017 Verification of CFD tool for simulation of cavitating flows in hydraulic systems. *Journal of Hydroinformatics* **19**, 653–665.

Powerchina ZhongNan Engineering Corporation Limited 2016 *Design Report of the Temperature-Control Curtain of Sanbanxi Reservoir in Guizhou.* Powerchina ZhongNan Engineering Corporation Limited, Changsha, China.

Sabag, S. R., Edge, B. L. & Soedigdo, I. 2000 Wake II model for hydrodynamic forces on marine pipelines including waves and currents. *Ocean Engineering* **27**, 1295–1319.

Shammaa, Y. & Zhu, D. Z. 2010 Experimental study on selective withdrawal in a two-layer reservoir using a temperature-control curtain. *Journal of Hydraulic Engineering* **136**, 234–246.

Shi, J. & Li, Y. 2016 Interface shear strength of textured geomembrane with nonwoven geotextile and change pattern of surface asperity. *Journal of Hohai University* **3**, 214–218. (In Chinese)

Soleimani, S., Bozorg-Haddad, O., Saadatpour, M. & Loaiciga, H. A. 2016 Optimal selective withdrawal rules using a coupled data mining model and genetic algorithm. *Journal of Water Resources Planning and Management* **142**, 0401606412.

Sun, J., Wang, R. & Duan, H. 2016 Multiple-fault detection in water pipelines using transient-based time-frequency analysis. *Journal of Hydroinformatics* **18**, 975–989.

Turcotte, B., Millar, R. G. & Hassan, M. A. 2016 Drag forces on large cylinders. *River Research and Applications* **32**, 411–417.

US Department of the Interior 2012 *Lewiston Temperature Management Intermediate Technical Memorandum*. US Dept. of the Interior, Washington, DC, USA.

Vermeyen, T. 1997 *Use of Temperature Control Curtains to Control Reservoir Release Water Temperatures. Report 97-09.* US Bureau of Reclamation, Denver, Colorado, USA.

Vermeyen, T. 2000 Application of Flexible Curtains to Control Mixing and Enable Selective Withdrawal in Reservoirs. In: *5th International Symposium on Stratified Flows*, 10–13th July, IAHR, Vancouver, Canada.

Wang, S. 2010 *Numerical and Experimental Investigation on the Interaction Between Moving Fluid and Flexible Bodies*. Thesis, University of Science and Technology of China, Anhui, China.

Wang, J., Fan, H. & Zhu, L. 2014 Experimental studies on tension and stability of a flexible dam. *Hydro-Science and Engineering* **5**, 1–7. (In Chinese)

Wang, H., Si, F., Lou, G., Yang, W. & Yu, G. 2015 Hydrodynamic characteristics of a suspended curtain for sediment trapping. *Journal of Waterway Port Coastal & Ocean Engineering* **141**, 040140301.

Wu, B., Wang, G., Liu, C. & Xu, Z. 2013 Modeling impacts of highly regulated inflow on thermal regime and water age in a shallow reservoir. *Journal of Hydroinformatics* **15**, 1312–1325.

Yang, S. & Lin, P. 2011 Coastal reservoir by soft-dam and its possible applications. *Recent Patents on Engineering* **5**, 45–56.

Younis, B. A., Teigen, P. & Przulj, V. P. 2001 Estimating the hydrodynamic forces on a mini TLP with computational fluid dynamics and design-code techniques. *Ocean Engineering* **28**, 585–602.

Zhang, S. & Gao, X. 2010 Effects of selective withdrawal on temperature of water released of Glen Canyon dam. In *4th International Conference on Bioinformatics and Biomedical Engineering (iCBBE)*, 18–20 June, Chengdu, China, pp. 1–4.

Zhu, L., Wang, J. & Fan, H. 2009 *Model Test Research on a Diversion Structures (Flexible, Activity and Suspended) Used for Xiaoshan Delivery Wharf in Hangzhou bay. Report*. Nanjing Hydraulic Research Institute, Nanjing, China.

First received 26 July 2017; accepted in revised form 30 November 2017. Available online 18 December 2017